Tridentate Nitrogen-Based Ligands in Cu-Based ATRP: A Structure−Activity Study

Krzysztof Matyjaszewski,* Bernd Göbelt, Hyun-jong Paik, and Colin P. Horwitz

Department of Chemistry, Carnegie Mellon University, 4400 Fifth Avenue, Pittsburgh, Pennsylvania 15213

Received July 10, 2000

ABSTRACT: The kinetic parameters for the activation and deactivation steps in ATRP for Cu-based catalysts were determined with eight different tridentate nitrogen-based ligands. Additionally, the redox properties of these Cu complexes were measured by cyclic voltammetry. By correlating the kinetic parameters of the activation and deactivation steps with the reduction potential of the Cu(II) complexes, it was found that more reducing Cu catalysts form faster activating Cu(I) and slower deactivating Cu(II) species. The rate of activation depends on the nature of the N-binding site of the ligand. Ligands with alkyl amine or pyridine binding sites form the fastest activating catalysts. The phenyl-substituted ligands form very slowly activating and very rapidly deactivating catalysts. Slower deactivation rates were found for catalysts with a central pyridine unit in the ligand than for catalysts derived from ligands with a central amine unit. In general, the activity of the ligands decreases in the following order: alkyl amine ≈ pyridine > alkyl imine ≫ aryl imine > aryl amine.

Introduction

Recently, extensive research has been carried out in the field of controlled/living radical polymerization.[1,2] Cu-based atom transfer radical polymerization (ATRP) is one of the most versatile and powerful techniques in this field.[3−5] In this polymerization method, the catalyst controls the polymerization reaction by mediating the atom transfer equilibrium shown in Scheme 1. In the activation step, with the rate constant k_{act}, a metal complex Mt^zL_mY cleaves the carbon−halogen bond of P_nX reversibly and homolytically, generating a carbon-centered radical species $P_n^{\bullet}$. The latter subsequently adds to the monomer with the rate constant k_p, before it is deactivated, with the rate constant k_{deact}, by the metal complex $XMt^{z+1}L_mY$ to form the dormant species P_nX. Through these reversible and repetitive cycles, well-defined polymers with high molecular weight are formed. Since the concentration of radicals is very low, termination often can be neglected.

Nitrogen-based polydentate ligands have been shown to be very efficient ligands for copper catalysts in terms of controlling the polymerization reaction. Thus, we recently focused on developing new catalytic systems employing such ligands. A wide range of monomers like (meth)acrylates, styrenes, acrylonitrile, acrylamides, and vinylpyridines have been polymerized and copolymerized successfully with Cu-based catalysts using ligands with amine, pyridine, or imine substructures.[6−26] These investigations revealed that the ligand played a crucial role in tuning the activity of the related catalyst in the activation and deactivation steps of the ATRP mechanism (Scheme 1). This equilibrium is affected by the electronic and steric effects of the ligand in the following ways. First, bulky ligands reduce the rate of activation, as the Cu center is harder to access for the bromine atom.[27] The second, and more predominant factor, is based mainly on the electronic interactions of the ligand with the Cu center in the complex. For example, good π-acceptor ligands efficiently stabilize the lower oxidation state of the metal center. This shifts the atom transfer equilibrium toward the dormant species P_nX. For example, when 2,2′-bipyridyl ligands with electron-withdrawing substituents, such as carbomethoxy groups at the 4,4′-positions, were used in Cu-catalyzed ATRP, the polymerization rate was significantly slower relative to polymerizations using unsubstituted 2,2′-bipyridine.[28]

Scheme 1. Mechanism of ATRP

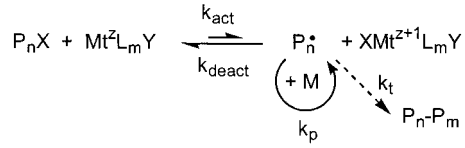

$$R_p = k_p \frac{k_{act}}{k_{deact}} [M][I]_0 \frac{[Cu^I]}{[XCu^{II}]} \quad (1)$$

$$\frac{M_w}{M_n} = 1 + \left(\frac{k_p[I]_0}{k_{deact}[XCu^{II}]}\right)\left(\frac{2}{p} - 1\right) \quad (2)$$

More precise descriptions about how the catalyst controls the polymerization through the atom transfer equilibrium are given in eqs 1 and 2. In these equations, $[I]_0$ refers to the initial concentration of the initiator. In eq 1, the rate of polymerization, R_p, is first order with respect to the monomer, [M], and the Cu(I) concentration, [Cu(I)], in solution. A high concentration of Cu(II), [XCu(II)], slows down the rate of polymerization. Not only does the rate constant of propagation, k_p, which is specific for each monomer, affect R_p, but also the rate constants for activation, k_{act}, and deactivation, k_{deact}. A high value for the ratio of k_{act}/k_{deact} gives a higher rate of polymerization as well. Equation 2 provides means for understanding how the molecular weight distribution, M_w/M_n, decreases with conversion, p. A narrower molecular weight distribution is obtained at higher conversion, higher k_{deact} relative to k_p, higher concentra-

* Corresponding author. E-mail km3b@andrew.cmu.edu; Fax 412-268-6897.

10.1021/ma001181s CCC: $20.00
Published on Web 01/03/2001

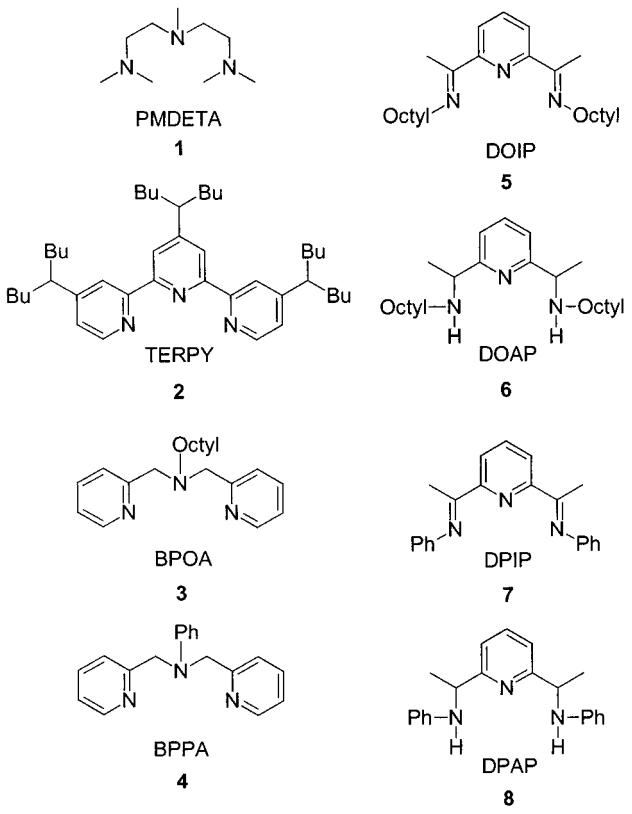

Figure 1. Linear tridentate ligands used in the structure–activity study.

tion of deactivator, and higher molecular weights, i.e., $1/[I]_0$. At the limit of a large k_{act} and a small k_{deact}, the desired high rate of polymerization is obtained, but ATRP simply becomes a conventional redox-initiated radical polymerization process resulting in a highly polydisperse polymer.

We are interested in determining how the ligand structure affects the activity of the copper catalysts in the polymerization reactions. Therefore, we conducted the structure–activity investigation for Cu catalysts with the linear tridentate ligands shown in Figure 1. The ligands possess five different types of N-binding sites: alkyl amine, aryl amine, alkyl imine, aryl imine, and pyridine units. We examined the effect of the ligands on the rates of activation and deactivation, and there appears to be a correlation between these parameters and the redox properties of the catalysts.

Results of the Polymerization Reactions

The results of the polymerization reactions with the CuBr complexes derived from the ligands **1**–**8** are listed in Table 1. Each catalyst polymerizes only a certain range of monomers. For example, CuBr/DOIP leads to a well-controlled polymerization reaction only for methyl methacrylate.[20] However, PMDETA or BPOA formed Cu catalysts suitable for the polymerization of a wider range of monomers based on (meth)acrylate and styrene derivatives.[10,14] In contrast, the polymerization reaction of methyl methacrylate with CuBr/DOAP was poorly controlled with a much higher experimental molecular weight ($M_{n(GPC)}$) than predicted ($M_{n(th)}$) and a relatively broad molecular weight distribution, M_w/M_n, of 1.6.[20] However, this catalyst enabled a well-controlled and fast polymerization of styrene. When using DPIP as a ligand in Cu-based ATRP, only a redox-initiated free radical polymerization of methyl methacrylate was obtained. In the case of CuBr/DPAP no polymerization of methyl methacrylate, styrene, or methyl acrylate occurred.[20]

Although the polymerization results provide information about the apparent activity of the catalyst, this is not an accurate measure of the activity due to the complexities of ATRP process. In addition to the catalyst activity, in the ATRP process, several other parameters such as the rate of termination reactions and the solubility of the catalyst also affect the rate of polymerization. As ATRP relies on the persistent radical effect[29] for controlling the polymerization reaction, a small amount of termination is required in order to build up the necessary Cu(II) concentration, unless Cu(II) is added at the beginning of the process. A catalyst that activates too quickly relative to its rate of deactivation generates a high concentration of radicals, which then terminate and form a high Cu(II) concentration. The consequence is a decrease in the polymerization rate (see eq 1). This effect was observed in the polymerization of methyl methacrylate with CuBr/DOAP. At 90 °C, the reaction was very slow, reaching a conversion of 73% in 22 h. At a lower temperature of 70 °C, the rate of the activation process is reduced, resulting in less termination and a faster polymerization (65% conversion after 7.25 h).[20]

The rate of polymerization is also affected by the relative solubilities of the activating and the deactivating species of the catalyst (Table 2). In heterogeneous systems, a low stationary concentration of the catalyst species allows for a controlled polymerization, but the polymerization is much slower than in homogeneous systems. An example is the bulk polymerization of methyl acrylate with CuBr/BPPA.[30] The low solubility of the Cu(I) species resulted in a slow polymerization reaction, only reaching 73% conversion in 15.5 h. The addition of 10% DMF improved the solubility of the catalyst in the polymerization solution. Thus, the reaction was faster, resulting in 60% monomer conversion in 3 h. Again, as the polymerization reaction is affected by several parameters, a direct comparison of the catalyst activity is not possible on the basis of the polymerization results. Therefore, we investigated the activities of the catalysts using model reactions for the activation and deactivation processes under homogeneous and identical conditions, using acetonitrile as a solvent.

Activation Study. The direct measurement of k_{act} was achieved by isolating the activation process (1) from the deactivation process (2) (Scheme 2). The radicals generated by halogen transfer to the copper complex (1) were scavenged with TEMPO. In the presence of a large excess of TEMPO (10 times with respect to the alkyl halide), it was expected that nearly all the alkyl radicals were trapped with TEMPO to form the corresponding alkyl–TEMPO adduct (3).[31] The deactivation step (2) can be ignored under the given conditions owing to the smaller rate constant (k_{deact})[32] and low $CuBr_2$ concentration. The contribution of the thermal decomposition of the alkyl TEMPO adduct (4) should be negligible at low reaction temperatures ($T = 35$ °C).[33] Reaction 5 can be also neglected due to the low radical concentration in the presence of an excess amount of the radical scavenger.

An excess of catalyst (about 10 times with respect to the concentration of the alkyl halide) was used to make

Table 1. Results of the Polymerization Reactions with the CuBr Catalysts Involved in This Study

catalyst	monomer	ratio $[M]_0$:$[I]_0$:$[cat]_0$	time (h)/temp (°C)	conv (%)	$M_{n(th)}$	$M_{n(GPC)}$	M_w/M_n
CuBr/PMDETA[10]							
	MMA	200:1:1	8.5/90	76	15 200	18 500	1.16
	styrene	96:1:1	2/110	90	9 000	8 500	1.23
	MA	232:1:1	2.5/90	92	18 500	16 400	1.11
CuBr/TERPY[18]							
	styrene	96:1:1	6/90	78	7 800	11 000	1.20
	MA	96:1:1	3/50	79	6 500	7 500	1.09
CuBr/BPOA[14]							
	MMA	200:1:1	8/50	73	14 500	22 900	1.18
	styrene	96:1:1	2/110	87	8 700	10 100	1.13
	MA	232:1:1	3/50	82	16 500	14 400	1.12
CuBr/BPPA[30]							
	styrene	96:1:1	3/110	67	6 700	4 200	1.77
	MA	232:1:1	15.5/90	64	12 800	13 800	1.28
CuBr/DOIP[20]							
	MMA	200:1:1	3.5/90	68	13 600	14 300	1.23
	styrene	200:1:1	13/110	55	11 400	13 000	1.74
	MA	200:1:1	20/90	15	2 600	6 300	1.43
CuBr/DOAP[20]							
	MMA	200:1:1	7.25/70	65	13 000	24 000	1.56
	styrene	200:1:1	5.3/110	73	15 200	22 000	1.18
	MA	200:1:1	15/90	62	10 700	9 200	1.26
(DPIP)CuBr[20]							
	MMA	200:1:1	redox-initiated free radical polymerization				
	styrene	200:1:1	no polymerization				
	MA	200:1:1	no polymerization				
CuBr/DPAP[20]							
	MMA	200:1:1	no polymerization				
	styrene	200:1:1	no polymerization				
	MA	200:1:1	no polymerization				

Table 2. Effects of Solvents and Temperature on the Rate of Polymerization

solvent	temp (°C)	time (h)	conv (%)	$M_{n(th)}$	$M_{n(GPC)}$	M_w/M_n
Termination Effect: CuBr/DOAP − Polymerization of MMA[a]						
50% anisole	90	22	73	14 600	26 800	1.83
50% anisole	70	7.25	65	13 000	24 000	1.56
Solubility Effect: CuBr/BPPA − Polymerization of MA[b]						
bulk	90	15.5	64	12 800	13 800	1.28
10% DMF	90	3	60	12 000	13 200	1.14

[a] $[MMA]_0$:$[CuBr/L]_0$:$[BPN]_0$ = 200:1:1. [b] $[MA]_0$:$[CuBr/L]_0$:$[MBP]_0$ = 232:1:1.

Scheme 2. Kinetic Isolation of the Activation Process

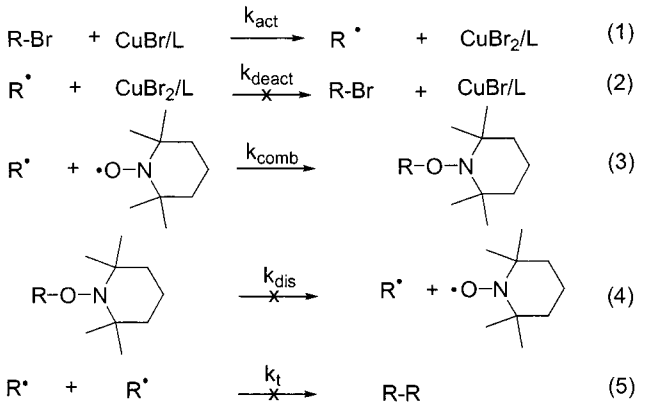

the kinetic analysis straightforward, i.e., to provide pseudo-first-order kinetic conditions. From the slope of the pseudo-first-order kinetic plot with respect to the concentration of the alkyl halide, the apparent rate constant of activation, k_{app}, was determined, which was the product of the catalyst concentration and the activation rate constant, k_{act} (eq 3). Similar approaches have been reported for the determination of the decomposition rate constants of alkyl−TEMPO adducts[33,34] and the activation reaction for model compounds[35,36] and polymeric chain ends.[37]

$$-\frac{d[RBr]}{dt} \approx k_{act}[Cu(I)Br/L][RBr] = k_{app}[RBr] \quad (3)$$

where $k_{act}[Cu(I)Br/L] = k_{app}$.

Previously, we reported that the activation rate constant could be measured using HPLC to monitor the consumption of benzyl bromide and 1-phenylethyl bromide in a CuBr/4,4′-di(5-nonyl)-2,2′-bipyridine (dNbpy) catalyzed reaction.[36] It was shown that the consumed alkyl bromide was almost equimolar to the formed alkoxyamine. This indicated that reaction 3 (in Scheme 2) was the major deactivation process and was much faster than the other processes, i.e., deactivation (2), termination (5), or other side reactions. Potential side reactions could involve the loss of hydrogen bromide[38] or the formation of hydroxylamine with the generation of an unsaturated product.[39,40] In our analysis, these side reactions were not taken into account since the relative rates of these side reactions are much slower than that of the trapping reaction (3).

HPLC analysis proved to be a reliable method for measurement of the activation rate constants for certain model compounds (i.e., UV-active alkyl halides). However, compounds such as EBiB and MBP (Figure 2) were difficult to analyze by HPLC due to their low extinction

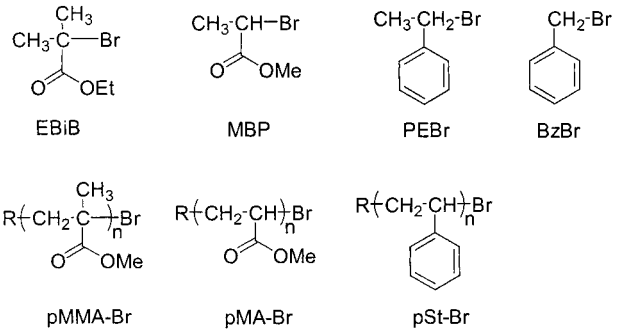

Figure 2. Model compounds for the activation study and their polymeric analogues.

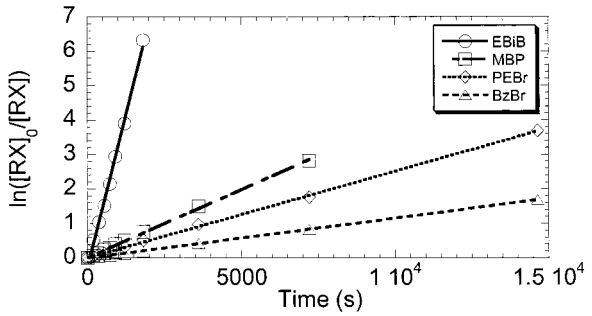

Figure 3. Kinetic plot of the activation experiment with the CuBr/DOAP catalyst at 35 °C in acetonitrile. $[CuBr/DOAP]_0 = 5 \times 10^{-3}$ M, $[I]_0 = 1 \times 10^{-4}$ M, $[TEMPO]_0 = 5 \times 10^{-3}$ M, and [biphenyl] $= 1 \times 10^{-4}$ M.

Table 3. Rate Constants of Activation for the Different Initiators and CuBr Complexes in Acetonitrile at 35 °C[a]

complex	EBiB [M^{-1} s^{-1}]	MBP [M^{-1} s^{-1}]	PEBr [M^{-1} s^{-1}]	BzBr [M^{-1} s^{-1}]
CuBr/PMDETA	1.8	0.15	0.1	0.13
CuBr/TERPY	1.5	0.41	0.42	0.38
CuBr/DOAP	0.7	0.08	0.05	0.023
CuBr/BPOA	0.3	0.014	0.066	0.066
CuBr/DOIP	0.1	0.011	0.014	0.0038
CuBr/BPPA	0.0057	0.0006	0.0014	0.0023
CuBr/DPIP	0.0009	0.0005	0.0004	0.0004
CuBr/DPAP	≅0.00009	≅0.000008	≅0.000002	≅0.000002

[a] $[CuBr/L]_0 = 5 \times 10^{-3}$ M, $[I]_0 = 10^{-4}$ M, $[TEMPO]_0 = 5 \times 10^{-3}$ M, and [biphenyl] $= 10^{-4}$ M.

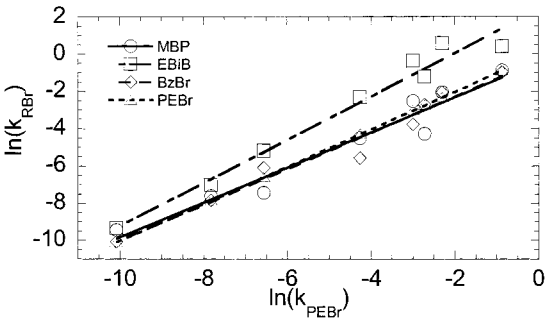

Figure 4. Bilogarithmic plot of the rates of activation for EBiB, MBP, BzBr, and PEBr vs PEBr. $[CuBr/L]_0 = 5 \times 10^{-3}$ M, $[I]_0 = 1 \times 10^{-4}$ M, $[TEMPO]_0 = 5 \times 10^{-3}$ M, and [biphenyl] $= 1 \times 10^{-4}$ M in acetonitrile, 35 °C.

coefficients. Subsequently, gas chromatography, GC, was found to be an attractive alternative method for these experiments owing to the high sensitivity and universal detection. Furthermore, several alkyl halides could be studied simultaneously in the same activation rate constant measurement, due to the sufficient separation of the substrates by GC. This approach allowed successful and expedient assaying of several model compounds representing dormant species in ATRP of various monomers.

Four alkyl halides were used as model compounds (Figure 2): ethyl 2-bromoisobutyrate (EBiB, model for polymethacrylate chain end), methyl 2-bromopropionate (MBP, model for polyacrylate chain end), 1-phenylethyl bromide (PEBr, model for polystyrene chain end), and benzyl bromide. These model compounds should have reactivities similar to the corresponding polymeric chain ends. However, in the case of EBiB, the reactivity could be lower than the pMMA chain end due to the B-strain effect, as previously discussed.[41,42]

The reaction was performed at 35 °C in acetonitrile in a Schlenk flask after degassing the solution by three freeze−pump−thaw cycles. The concentration of each alkyl bromide was 1×10^{-4} M, and the concentration of CuBr/L was 5×10^{-3} M to provide the pseudo-first-order kinetic condition. The TEMPO concentration was 5×10^{-3} M so that essentially all the generated radicals could be trapped during the reaction. The approximate linearity of the first-order kinetic plot with respect to the concentration of alkyl halide supported the above assumptions (Figure 3).

Not surprisingly, the CuBr complexes which form highly active ATRP catalysts in the polymerization reactions are fast activating species in this model study (Table 3). Specifically, Cu(I) complexes with ligands derived from alkyl amine and pyridine structures activate quickly. The homoleptic ligands PMDETA and TERPY form faster activating catalysts than their related mixed pyridine−amine analogues DOAP and BPOA. The change from alkyl-substituted amine moieties in the diaminopyridine ligand, DOAP, to imine moieties in the diminopyridine ligand, DOIP, results in a slower activating catalyst. In contrast to the high activity in the polymerization reactions, CuBr/BPPA has a relatively low rate of activation for the four initiators used in the model study. The explanation for this discrepancy in activity for the BPPA complex is the poor solubility of the Cu(II) species in the nonpolar polymerization medium, which shifts the atom transfer equilibrium toward the active side by suppressing the deactivation, as described above. Slow rates of activation were also measured for the Cu(I) complexes of the other phenyl-substituted ligands DPIP and DPAP. The trends in the changes of the rates of activation for the different initiators are illustrated in Figure 4. Here, the activation rate constants for four initiators are plotted vs k_{act} for PEBr on a bilogarithmic scale (Figure 4). The linearity of the data indicates that for all catalysts and initiators the activation process occurs via the same mechanism. In principle, for all Cu(I) complexes the rate constants of activation for MBP, PEBr, and BzBr are similar (Figure 4). In comparison, with these three initiators the EBiB activation is significantly faster (Figure 4). We attribute this difference to the higher stability of the radical formed from EBiB in the activation step and higher reactivity of alkyl halide species.

Deactivation Study. The most reliable way to determine the rate constants for very fast radical reactions would be to measure the radical concentration with spectroscopic techniques after photogeneration of radical. However, in a metal-catalyzed reaction, the absorption bands from the metal complex often interfere with this approach. In the case of metal-catalyzed ATRP or ATRA (atom transfer radical addition), the strong

Scheme 3. Model Reaction for the Deactivation Experiment

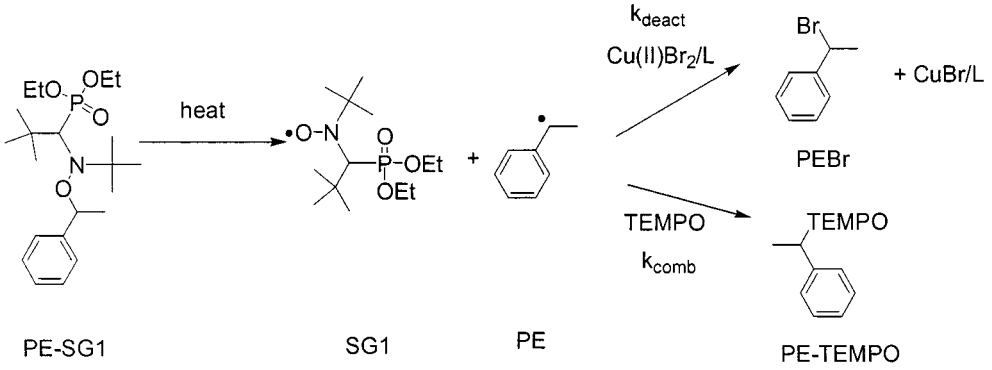

color of the solution limits the use of the photochemical reaction and quantification by spectroscopy. Therefore, the deactivation rate constant was measured using radical trapping with TEMPO as a clock reaction. The coupling of alkyl radicals with TEMPO is both a well-known and well-calibrated radical reaction.[43,44] In the present case, the radicals could react with either TEMPO or $CuBr_2$/L forming an alkoxyamine or an alkyl bromide, respectively. By comparing the amount of the two products formed, the deactivation rate constant has been calculated:

$$\frac{d[PEBr]}{d[PETEMPO]} = \frac{k_{deact}}{k_{comb}} \frac{[Cu(II)Br_2/L][PE^*]}{[TEMPO][PE^*]} \quad (4a)$$

$$k_{deact} = k_{comb} \frac{[TEMPO]}{[Cu(II)Br_2/L]} \frac{d[PEBr]}{d[PETEMPO]} \quad (4b)$$

The 1-phenylethyl radical (PE) was generated by thermolysis of the 1-(*N*,*N*-(2-methylpropyl-1)-(1-diethylphosphono-2,2-dimethylpropyl-1-)-*N*-oxyl)-1-phenylethane (PESG1) as shown in Scheme 3. PESG1 was chosen as a radical source for two reasons. First, the decomposition of PESG1 was much faster than that of the TEMPO adduct, providing a sufficient concentration of radicals at relatively low temperature (75 °C) with minimum decomposition of the produced TEMPO adduct. Second, since the coupling between PE and SG1 is slower than with TEMPO or the $CuBr_2$/L under the reaction conditions, the interference of SG1 could be suppressed.[45] The reaction mixture was analyzed using reversed-phase HPLC.[46] The aromatic chromophore in the products (PEBr and PETEMPO), as well as the reactant (PESG1), allowed for sensitive quantification by UV detection (220 nm). The formation of PEBr and PETEMPO were monitored at the same time (Figure 5). The literature value of k_{comb} of 1.3×10^8 M^{-1} s^{-1} was used for the calculation of k_{deact}[47] (Table 4). The small decrease of the ratio [PEBr]/[PETEMPO] is due to the decomposition of PEBr[38] and to the reactivation of PEBr with Cu(I)Br/L. The rate constants of deactivation for the 1-phenylethyl radical range from 4.1×10^5 M^{-1} s^{-1} for the slowly deactivating $CuBr_2$/TERPY to 7.2×10^7 M^{-1} s^{-1} for the rapidly deactivating $CuBr_2$/DPAP. The rate constant of deactivation depends on the ligand as in the case of the activation rate. The comparison of the rate constants of deactivation with the rate constants of activation led to the general trend that Cu catalysts, which activate quickly, deactivate slowly, and the converse applies as well.

However, in addition to this overall deactivation trend, a second and weaker effect was observed for the case of the five ligands, which do not bear phenyl substituents. $CuBr_2$/PMDETA and $CuBr_2$/BPOA, which contain a central amine binding site, deactivated significantly faster than Cu(II) complexes derived from ligands with a central pyridine unit like $CuBr_2$/TERPY and $CuBr_2$/DOAP. The diiminopyridine complex $CuBr_2$/DOIP confirms this behavior too, as $k_{deact} = 3.1 \times 10^6$ M^{-1} s^{-1} is slower than those for $CuBr_2$/PMDETA ($k_{deact} = 6.1 \times 10^6$ M^{-1} s^{-1}) and for $CuBr_2$/BPOA ($k_{deact} = 3.3 \times 10^6$ M^{-1} s^{-1}). This was not expected, since in the activation study, the DOIP catalyst was identified as a slower activator than the PMDETA- or BPOA-based catalysts, and for $CuBr_2$/DOIP a higher k_{deact} was predicted than for either $CuBr_2$/PMDETA or $CuBr_2$/BPOA. This structural comparison of the Cu(II) catalyst leads to the conclusion that the central N-binding site of the ligand has a more significant effect on the rate of deactivation.

This effect was less clear in the case of the phenyl-substituted N-binding sites, which have a high rate of deactivation regardless of their positions in the ligand.

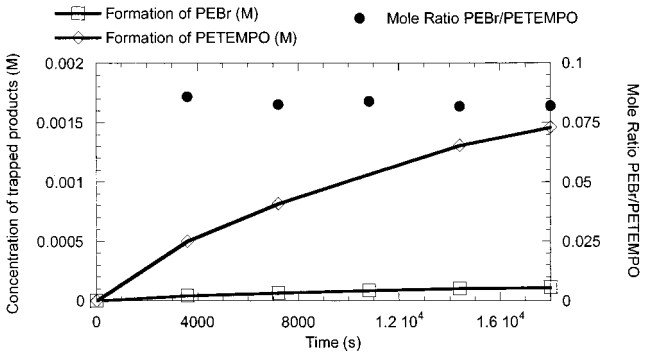

Figure 5. Formation of trapping products and their ratio in the deactivation experiment with $CuBr_2$/BPPA, TEMPO, and PESG1. $[CuBr_2/L]_0 = [TEMPO]_0 = [PESG1]_0 = 2 \times 10^{-3}$ M and [biphenyl] $= 6 \times 10^{-4}$ M in acetonitrile, 75 °C.

Table 4. Rate Constants of Deactivation k_{Deact} for the Different $CuBr_2$ Complexes with PESG1

complex	k_{deact} [M^{-1} s^{-1}]	complex	k_{deact} [M^{-1} s^{-1}]
$CuBr_2$/TERPY[a]	4.1×10^5	$CuBr_2$/PMDETA[b]	6.1×10^6
$CuBr_2$/DOAP[a]	4.2×10^5	$CuBr_2$/DPIP[c]	7.9×10^6
$CuBr_2$/DOIP[a]	3.1×10^6	$CuBr_2$/BPPA[c]	9.1×10^6
$CuBr_2$/BPOA[a]	3.3×10^6	$CuBr_2$/DPAP[c]	7.2×10^7

[a] $[CuBr_2/L]_0 = 2 \times 10^{-2}$ M, $[TEMPO]_0 = 6 \times 10^{-3}$ M, $[PESG1]_0 = 2 \times 10^{-3}$ M, [biphenyl] $= 6 \times 10^{-4}$ M in acetonitrile, 75 °C. [b] $[CuBr_2/L]_0 = 10^{-2}$ M, $[TEMPO]_0 = 6 \times 10^{-3}$ M, $[PESG1]_0 = 2 \times 10^{-3}$ M, [biphenyl] $= 6 \times 10^{-4}$ M in acetonitrile, 75 °C. [c] $[CuBr_2/L]_0 = [TEMPO]_0 = [PESG1]_0 = 2 \times 10^{-3}$ M, [biphenyl] $= 6 \times 10^{-4}$ M in acetonitrile, 75 °C.

Table 5. Redox Potentials of the CuBr and $CuBr_2$ Complexes of the BPOA Ligand Measured by Cyclic Voltammetry at 500 mV/s in Acetonitrile (*E* vs SSCE)[a]

entry	BPOA complex	E_{red} [mV]	E_{ox} [mV]	$E_{1/2}$ [mV]
1	CuBr (prev study)[49]	−135	70	−33
2	CuBr (this study)	−145	30	−60
3	CuBr + Br^-	−170	−45	−108
4	$CuBr_2$	−175	−30	−103

[a] $[CuBr_2/L]_0 = 0.01$ M, 0.1 M [*n*-Bu_4N][PF_6], room temperature. For $[Cp_2Fe]^{0/+}$, $E_{1/2} = 395$ mV, $\Delta E_p = 65$ mV.

Here, $CuBr_2$/DPAP with a central pyridine unit deactivated 8 times faster than $CuBr_2$/BPPA with a central phenyl amine binding site.

Electrochemical Study. An examination of the electrochemical properties of the Cu complexes was conducted to correlate their redox properties with the kinetic parameters of the activation and deactivation steps. Previously, we discussed the importance of outer-sphere electron transfer (OSET) in ATRP and roughly correlated the electrochemical properties of some Cu complexes with their activity as ATRP catalysts in the polymerization of methyl acrylate.[48,49] Generally, in determining a correlation between electrochemical properties and kinetic parameters, we have to take into account that the two processes can occur via different electron-transfer mechanisms. ATRP involves a concerted inner-sphere electron-transfer process (ISET, also called atom transfer) between the organic halide and the metal complex (eq 5). However, a two-step process with an outer-sphere electron transfer (OSET) followed by halide migration is also possible (eq 6).

inner-sphere electron-transfer process (ISET)

$$R{-}X + M_t^{\,n}L_m \rightleftharpoons [R{---}X{---}M_t^{\,n}L_m] \rightleftharpoons R^\bullet + X{-}M_t^{\,n+1}L_m \quad (5)$$

outer-sphere electron-transfer process (OSET)

$$R{-}X + M_t^{\,n}L_m \rightleftharpoons [RX^{-\bullet} \rightarrow R^\bullet + X^-] + M_t^{\,n+1}L_m \rightleftharpoons R^\bullet + X{-}M_t^{\,n+1}L_m \quad (6)$$

This situation becomes even more complicated because apparently the electrochemical behavior of the copper complexes may be dependent on which oxidation state the compound is initially used. In our previous study, the cyclic voltammograms were recorded starting from Cu(I) complexes prepared in situ. In this study, we used isolated and characterized $CuBr_2$ complexes. More negative reduction and oxidation potentials were obtained when the Cu(II) complexes were used instead of the Cu(I). Therefore, we used the BPOA complexes to examine in detail this difference in electrochemical behavior (Table 5).

The cyclic voltammogram of the CuBr/BPOA complex was used as a check, and the oxidation potentials were found to be close to the previously published ones (Table 5, entries 1 and 2; the $[Cp_2Fe]^{0/+}$ couple is at 395 mV, $\Delta E_p = 65$ mV under our measurement conditions).[49] The cyclic voltammogram of the $CuBr_2$/BPOA complex gave a reduction wave at −175 mV, which is slightly lower than for the CuBr/BPOA cyclic voltammograms (−135 and −145 mV). The oxidation wave in the $CuBr_2$/BPOA cyclic voltammogram is at −30 mV compared to 30 and 70 mV for the CuBr/BPOA cyclic voltammograms. Possible explanations for this behavior lie in the different coordination spheres of the starting Cu(I) and Cu(II) complexes and the role of the counterion. For CuBr/BPOA, the cycle starts with the oxidation of the initial Cu(I) complex to Cu(II). This Cu(II) complex has only one bromide. The positive charge has to be compensated for by PF_6^- anions of the electrolyte. On the other hand, the redox cycle for $CuBr_2$/BPOA starts with its reduction to the Cu(I) species. It is not known that if one bromide was detached during the electron transfer or if a $[(BPOA)CuBr_2]^-$ species was formed first and then bromide loss occurred in a second step. Further investigation into this phenomenon showed that, with the addition of an excess of a bromide source such as [NBu_4]Br, the cyclic voltammogram of CuBr/BPOA was transformed into a $CuBr_2$-like cyclic voltammogram (Figure 6).

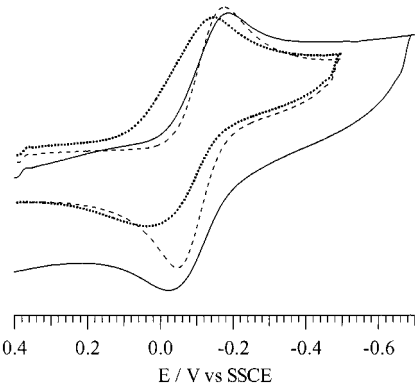

Figure 6. Cyclic voltammograms in CH_3CN of CuBr/BPOA, entry 2 (· · ·), CuBr/BPOA + Br, entry 3 (- - -), and $CuBr_2$/BPOA, entry 4 (—). 500 mV/s, 0.1 M [NBu_4][PF_6], *E* vs SSCE.

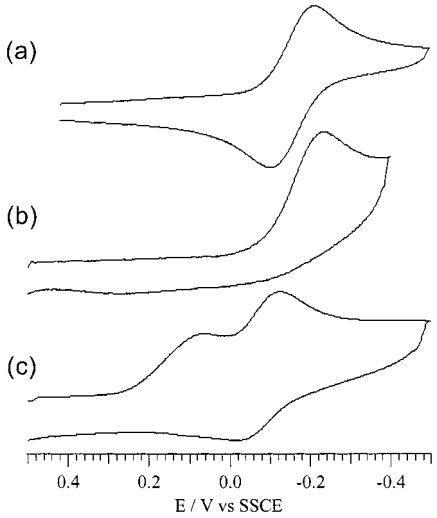

Figure 7. Observed types of cyclic voltammograms in CH_3CN: (a) quasi-reversible ($CuBr_2$/DOAP), (b) irreversible ($CuBr_2$/TERPY), (c) two, one-electron reduction of $CuBr_2$/DPIP, 500 mV/s, 0.1 M [NBu_4][PF_6], *E* vs SSCE.

The $CuBr_2$ complexes basically showed three different types of cyclic voltammograms (Figure 7). All the redox cycles are quasi-reversible or irreversible. In the quasi-reversible cases, the reduction wave (Cu(II) → Cu(I)) and the corresponding oxidation wave (Cu(I) → Cu(II)) were observed (Figure 7a). The cyclic voltammogram in Figure 7a is described as quasi-reversible because the ΔE_p values, which are defined as ($E_{red} - E_{ox}$), are larger than the ideal 60 mV,[50] and the ΔE_p increases with increasing scan rate. For some complexes, only a reduction wave was detected, and no oxidation wave appeared prior to the oxidation of Br^- (Figure 7b). The diiminopy-

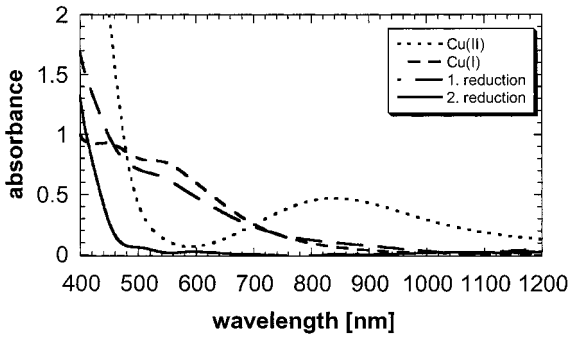

Figure 8. UV/vis spectra of $CuBr_2$/DPIP (· · ·), CuBr/DPIP (- - -), and $CuBr_2$/DPIP after the reduction with 1 (- -) and 2 equiv (—) of Cp_2Co, $[complex]_0 = 0.01$ M, acetonitrile, room temperature.

Table 6. Redox Potentials of the $CuBr_2$ Complexes[a]

Cu(II) complex	E_{red} [mV]	E_{ox} [mV]	$E_{1/2}$ [mV]
TERPY[b]	−240		
PMDETA	−155	−45	−100
BPOA	−175	−30	−103
BPPA	70	190	130
DOAP	−220	−100	−160
DPAP	200	340	270
DOIP[c]	−110		
DPIP[c]	65		

[a] Measured by cyclic voltammetry at 500 mV/s in acetonitrile at room temperature, E vs SSCE, $[CuBr_2/L]_0 = 0.01$ M, 0.1 M [n-Bu_4N][PF_6]. [b] Irreversible cycle. [c] Irreversible cycle for the Cu reduction and oxidation and a second reversible reduction and corresponding oxidation were observed.

ridine complexes $CuBr_2$/DOIP and $CuBr_2$/DPIP exhibited unique electrochemical behavior (Figure 7c). Both complexes exhibited two relatively closely spaced one-electron reductions, and only the more negative one had a corresponding oxidation wave. To determine which reduction wave was associated with the reduction of Cu(II), a chemical reduction of $CuBr_2$/DPIP with Cp_2Co ($E_{1/2} = -0.86$ V vs SCE in CH_2Cl_2)[51] was performed and monitored by UV/vis spectroscopy. With this chemical reduction, we could simulate the redox process in the cyclic voltammetry. The reaction with 1 equiv of Cp_2Co reduces the species with more positive E_{red} potential. After adding the first equivalent of Cp_2Co, the absorption of the Cu(II) complex at 834 nm disappeared completely, and a shoulder at 540 nm appeared (Figure 8). A comparison of the UV/vis spectra obtained after the reduction of $CuBr_2$/DPIP with an authentic sample of CuBr/DPIP indicates clearly that the Cu(I) complex was formed in the reduction. Therefore, in the cyclic voltammogram the more positive reduction wave belongs to the Cu(II) reduction. A second reducing equivalent generated a spectrum lacking any absorption in the visible region of the spectrum (Figure 8).

The results of the cyclovoltammetric measurements are listed in Table 6. The ligand has two effects on the electrochemical behavior of the corresponding Cu(II) complexes. The first one is illustrated in Figure 9 where the reduction potentials of the Cu(II) complexes are placed on a potential axis. It is possible to separate the complexes into two groups based on their reduction potentials. The Cu(II) complexes derived from the phenyl-attached ligands have positive reduction potentials (65−200 mV), indicating that they form Cu complexes that are relatively easy to reduce to Cu(I) and also difficult to oxidize to Cu(II). Correspondingly, these complexes have a low activity in ATRP. The Cu complexes which are active catalysts in ATRP are much easier to oxidize and have low oxidation (−30 to −100 mV) and reduction potentials (−240 to −110 mV). As in the deactivation study, it is possible to separate the Cu(II) complexes of the ligands TERPY, DOAP, PMDETA, and BPOA into two different groups on the basis of the nature of the central N-binding site of the ligand. The $CuBr_2$/PMDETA and $CuBr_2$/BPOA complexes having a central amine binding site in the ligand structure are reduced at more positive potential than the $CuBr_2$/$DOAP_2$ and $CuBr_2$/TERPY complexed which have a central pyridine unit. This indicates that in these complexes the central N-binding site tunes the reduction potential.

Discussion

The activation and deactivation studies described above provide information about the kinetic parameters of the atom transfer equilibrium while the electrochemical study describes the thermodynamic stability of the Cu(I) and Cu(II) complexes. Previously, a linear, semilogarithmic correlation of the redox potential of the Cu complexes with various nitrogen-based ligands, and their apparent equilibrium constant in ATRP of methyl acrylate was found.[49] In the present study, the reduction potentials, E_{red}, were taken instead of the redox potentials, $E_{1/2}$, because only five oxidation potentials of the eight complexes could be determined in the electrochemical study. Naturally, the reduction potential refers to the deactivation step in the atom transfer equilibrium, as both describe the change from Cu(II) to Cu(I). However, a linear correlation was found, when both k_{act} and k_{deact} were plotted vs the reduction potential (Figure 10). It can be seen that the more negative the Cu(II) reduction potential, the greater the rate of activation. Conversely, the rate of deactivation decreases as the Cu(II)−Cu(I) process becomes more negative. The activity of the catalyst can be described by the ratio (k_{act}/k_{deact}). This is not the true equilibrium constant, because the rates of activation and deactivation were determined at different temperatures (35 and 75 °C, respectively). However, the increase in $\ln(k_{act}/k_{deact})$ as the Cu(II) reduction potential becomes more negative indicates that the Cu catalysts become more active for ATRP.

According to the Hammond postulate, the effect of ligands on the fast exothermic deactivation process should be smaller than on the slow endothermic activation process. However, as shown in Figure 10, ligands affect both reactions to nearly the same extent. This can be partially explained by much larger variation of the complexation constants between various ligands and Cu(II) than Cu(I), as recently described for related systems.[52]

The $CuBr_2$ complexes of TERPY and DOAP deactivate approximately 10 times slower than the related $CuBr_2$ complexes of PMDETA and BPOA, as shown in Figure 11. Correspondingly, TERPY and DOAP ligands form Cu(II) complexes which are harder to reduce than the PMDETA and BPOA Cu(II) complexes. It appears that ligand flexibility is important. Rigid TERPY and DOAP force Cu(I) complex in the square-planar structure and Cu(II) in the distorted trigonal-bipyramidal structure. For more flexible PMDETA and BPOA, Cu(I) can easier adopt tetrahedral structure, but Cu(II) is in distorted square-pyramidal configuration.[53] Cu(I) prefers tetrahedral and Cu(II) prefers trigonal-bipyramidal structure, accessible for PMDETA and TERPY complexes,

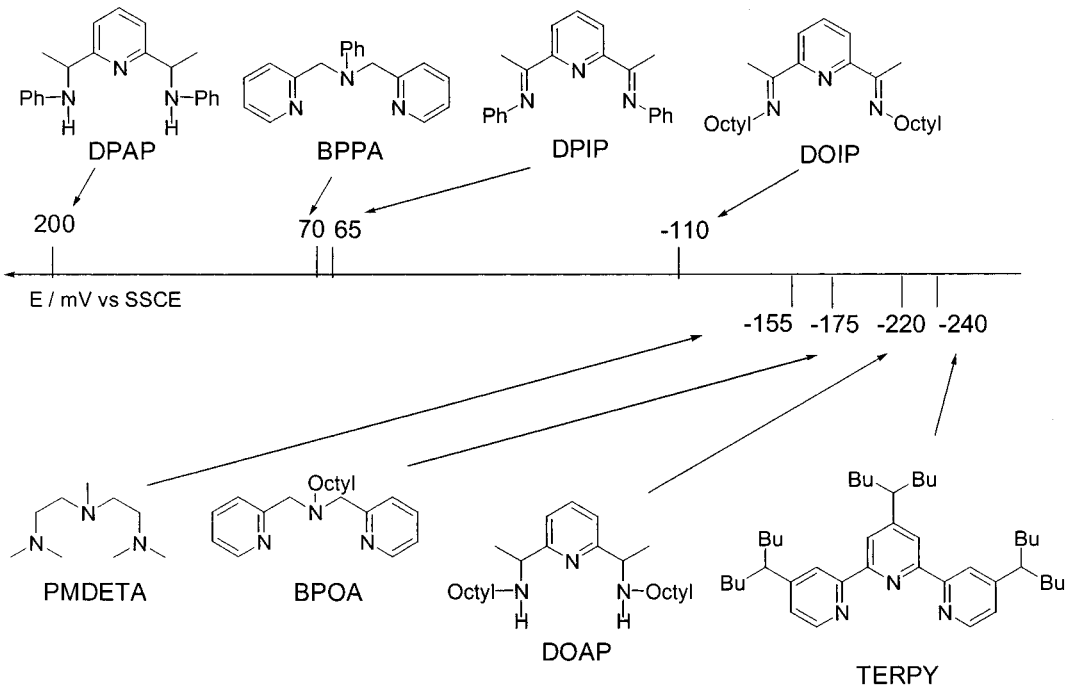

Figure 9. Reduction potentials of the $CuBr_2$ complexes in CH_3CN, 500 mV/s, 0.1 M $[NBu_4][PF_6]$, E vs SSCE.

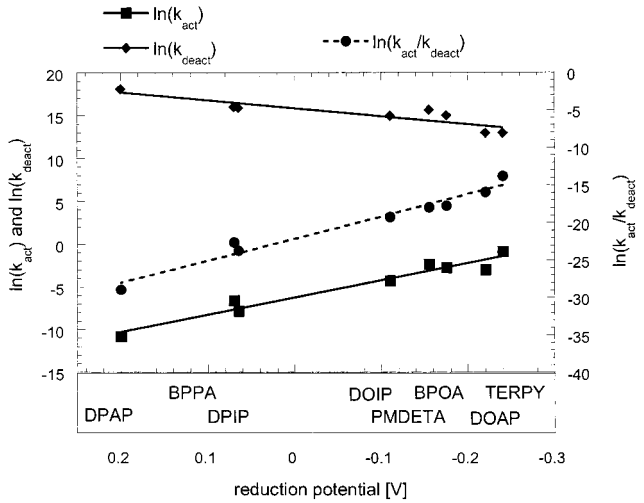

Figure 10. Dependence of the rate of activation for PEBr and deactivation for PESG1 as well as their ratio (k_{act}/k_{deact}) on the reduction potential of the Cu(II) complexes. Rate constants of activation and deactivation were determined in acetonitrile at 35 and 75 °C, respectively.

respectively. This correlates with faster deactivation for Cu(II)/PMDETA and much slower for Cu(II)/TERPY, since the latter exists in a structure preferred for Cu(II) complexes. It also seems that the central nitrogen binding site (pyridines in TERPY and DOAP vs alkyl amine in PMDETA and BPOA) might have a tuning effect on the deactivation rates, which can originate in the Jahn−Teller effect.[54,55]

Since the ligands influence the activation and deactivation behavior of the Cu catalysts through their electronic interactions with the Cu center, it is possible to classify the ligands based on different N-binding sites (Figure 12). Generally, the phenyl-substituted ligands form very slowly activating and very rapidly deactivating Cu catalysts for ATRP. The phenyl groups attached to the N-binding sites stabilize the Cu(I) state. Therefore, these complexes possess an activity that is not sufficient for ATRP.

A comparison of the effect of pyridines and imines as ligands on the stabilization of metals in low oxidation states by tom Dieck et al. revealed that π-back-bonding is twice as strong for α-diimines as compared to 2,2′-bipyridines.[56] This results in better stabilization of the lower oxidation states of a metal center when complexed with α-diimines rather than with 2,2′-bipyridines. The same effect was observed when the stability of the Cu(I) and Cu(II) complexes of the diiminopyridine ligand, DOIP, and the terpyridine ligand, TERPY, were compared. The reduction potentials of $CuBr_2$/DOIP and $CuBr_2$/TERPY of −110 and − 240 mV, respectively, clearly indicate that the DOIP ligand stabilizes a Cu(I) center better than the related terpyridine ligand, which forms a very stable Cu(II) complex. Therefore, a slow activation and a fast deactivation are found for the DOIP Cu complex. This activation−deactivation activity of the DOIP-based catalyst is optimal for the controlled polymerization of methyl methacrylate (see Table 1) but too low for the polymerization of styrene or methyl acrylate.

The rapid activators formed with the ligands PMDETA, BPOA, TERPY, and DOAP can be separated in two different groups on the basis of their rates of deactivation. PMDETA and BPOA form rapidly deactivating catalysts. TERPY and DOAP form slowly deactivating catalysts. These differences affect the polymerization reactions because the molecular weight distribution is influenced by the rate of deactivation (eq 2). Therefore, a sufficiently high rate of deactivation is required in order to obtain a well-controlled polymerization. This can be illustrated by comparing the rapidly deactivating PMDETA-based Cu catalyst with the slowly deactivating DOAP-based Cu catalyst. CuBr/PMDETA is a suitable ATRP catalyst for a fast polymerization of methyl methacrylate giving a narrow molecular weight distribution ($M_w/M_n = 1.16$) and experimental molecular weights that match relatively well with the predicted ones ($M_{n(GPC)} = 18\,500$ and $M_{n(th)} = 15\,200$). When CuBr/DOAP was used for the methyl methacrylate polymerization, a molecular weight distribution of 1.56 and a

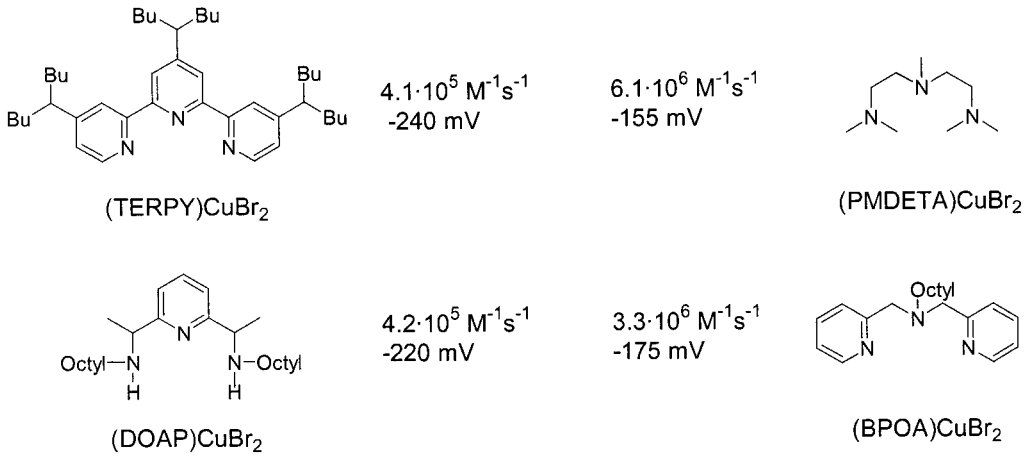

Figure 11. Dependence of the rate of deactivation and reduction potential of the Cu(II) complexes on the nature of the central N-binding site.

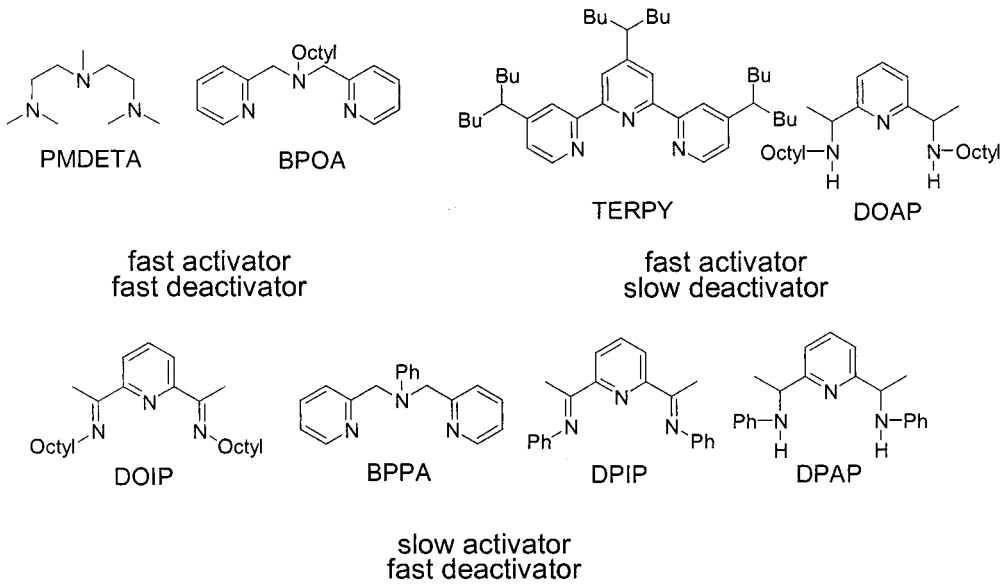

Figure 12. Effects of the ligands on the rate of activation and deactivation of their related Cu complexes.

much higher experimental molecular weight than predicted was obtained ($M_{n(GPC)}$ = 24 000 and $M_{n(th)}$ = 13 000). These differences in the polymerization reactions reflect the different rates of deactivation for the two catalysts. This suggests that PMDETA and BPOA are suitable ligands for the Cu-based ATRP of a wide range of monomers of (meth)acrylate and styrene types. The slowly deactivating TERPY- and DOAP-based Cu catalysts do not fulfill the fast deactivation requirement for a well-controlled polymerization and are therefore less suitable for ATRP.

Conclusion

The present study provided the first systematic evaluation of the activation and deactivation processes in ATRP. Copper complexes with eight different linear, tridentate nitrogen-based ligands with phenyl- and alkyl-substituted imine and amine units as well as pyridine units were studied in model activation and deactivation processes. Generally, a slowly activating catalyst deactivates quickly, and a rapidly activating catalyst deactivates slowly. Additionally, in the deactivation study, a dependence of k_{deact} on the central N-binding site was found for some Cu complexes. This allows for the separate tuning of k_{act} and k_{deact} with the ligand structure. An ideal ATRP catalyst should have very large k_{deact} and appropriate k_{act}. An understanding of various effects of ligands on the dynamics of ATRP will enable one to prepare such catalysts. The comparison of the kinetic parameters of the atom transfer equilibrium with the redox properties of the Cu complexes gave a linear, semilogarithmic correlation. This indicates that the catalyst becomes more active when the Cu(II) state of the catalyst is better stabilized by the ligand. In general, the activity of the ligands decreases in the following order:

$$\text{alkyl amine} \approx \text{pyridine} > \text{alkyl imine} \gg \text{aryl imine} > \text{aryl amine}$$

Ligands derived from pyridine and alkyl amine units like the triamine ligand PMDETA, the terpyridine ligand TERPY, the bis(picolyl)amine ligand BPOA, and the diaminopyridine ligand DOAP form highly active catalysts. The incorporation of alkyl imine units, like in the diiminopyridine ligand DOIP, decreases the activity of the catalyst compared with the TERPY- or the DOAP-based catalysts. Ligands with phenyl-substituted imine and amine units form nonactive ATRP catalysts.

Experimental Part

Materials. *N,N*-(2-Methylpropyl-1)-(1-diethylphosphono-2,2-dimethylpropyl-1-)-*N*-oxyl (SG1) was provided by Elf Atochem. CuBr was stirred in glacial acetic acid under argon, filtered, washed with absolute ethanol, and dried. The ligands 1-(2,2,6,6-tetramethylpiperidinyloxy)-1-phenylethane (PETEMPO)[31] and 1-(*N,N*-(2-methylpropyl-1)−(1-diethylposphono-2,2-dimethylpropyl-1-)-*N*-oxyl)-1-phenylethane (PESG1)[45] were prepared according to literature procedures. All other chemicals were used as purchased from Aldrich.

Synthesis of the Cu(II) Complexes. One millimole of ligand in 10 mL of acetone was added slowly to 1 mmol of $CuBr_2$ in 10 mL of acetone. The color of the solution changed immediately to green or brown (DPIP). After 1 h of stirring the solution was passed through a pad of Celite. After evaporation of the solvent the product was washed with Et_2O. Yield: 80−95%.

(TERPY)$CuBr_2$: Anal. Calcd for $C_{42}H_{65}Br_2CuN_3$: C, 60.39; H, 7.84; N, 5.03. Found: C, 60.10; H, 7.83; N, 5.13.

(PMDETA)$CuBr_2$: Anal. Calcd for $C_9H_{23}Br_2CuN_3$: C, 27.25; H, 5.84; N, 10.59. Found: C, 27.53; H, 5.80; N, 10.32.

(BPOA)$CuBr_2$: Anal. Calcd for $C_{20}H_{29}Br_2CuN_3$: C, 44.92; H, 5.47; N, 7.86. Found: C, 45.05; H, 5.25; N, 7.67.

(BPPA)$CuBr_2$: Anal. Calcd for $C_{18}H_{17}Br_2CuN_3$: C, 43.35; H, 3.44; N, 8.43. Found: C, 43.02; H, 3.22; N, 8.39.

(DOAP)$CuBr_2$: Anal. Calcd for $C_{25}H_{47}Br_2CuN_3$: C, 48.98; H, 7.73; N, 6.85. Found: C, 48.71; H, 7.69; N, 6.64.

(DOIP)$CuBr_2$: Anal. Calcd for $C_{25}H_{43}Br_2CuN_3$: C, 49.31; H, 7.12; N, 6.90. Found: C, 49.48; H, 6.88; N, 6.66.

(DPAP)$CuBr_2$: Anal. Calcd for $C_{21}H_{23}Br_2CuN_3$: C, 46.64; H, 4.29; N, 7.77. Found: C, 46.16; H, 4.03; N, 7.20.

(DPIP)$CuBr_2$: Anal. Calcd for $C_{21}H_{19}Br_2CuN_3$: C, 46.99; H, 3.57; N, 7.83. Found: C, 46.82; H, 3.54; N, 8.02.

Polymerization Experiments. A detailed procedure for the polymerization was previously reported.[20]

Activation Experiments. The Cu(I) complexes were prepared in situ under an N_2 atmosphere by adding 9 mL of deoxygenated acetonitrile to 5×10^{-2} mmol of ligand, 7.8 mg of TEMPO, and 7.2 mg of CuBr in a Schlenk flask. After stirring for 30 min at 35 °C, 1 mL of deoxygenated substrates stock solution (EBiB, MBP, PEBr, BzBr, and biphenyl, 1.0×10^{-3} M each) were added to the Schlenk flask via a degassed syringe. A sample was taken immediately for the reference, and other samples were taken at timed intervals to measure kinetics. The samples were passed through alumina in order to remove the catalyst. The composition of the samples was analyzed by gas chromatography, which was performed using Shimadzu GC-17A, AOC-20i autosampler, and a J&W Scientific DB 608 column (30 m × 0.53 mm) with a FID detector. The injector and detector temperature was kept constant at 250 °C. The temperature program for the GG column was as follows: initial temperature 45 °C, 0 min; ramp 5 °C/min; final temperature 180 °C, 0 min. The retention times of MBP, EBiB, PEBr, BzBr, biphenyl, and TEMPO were 4.2, 5.5, 12.1, 10.8, 18.8, and 10.3 min, respectively. The data were collected and processed with a Shimadzu Class VP chromatographic data system (version 4.2).

Deactivation Experiments. To 6.7 mg of $CuBr_2$ and 3×10^{-2} mmol of a ligand in 2.40 mL of acetonitrile were added 0.30 mL of TEMPO stock solution (0.030 M in acetonitrile) and 0.30 mL of PESG1 and biphenyl stock solution (0.010 M each in acetonitrile). The solution was deoxygenated with three "freeze−pump−thaw" cycles. After taking a sample, the solution was heated to 75 °C in an oil bath, and samples were taken at timed intervals. The samples were passed through alumina in order to remove the catalyst. The concentration of PEBr, PESG1, and PETEMPO was determined using reversed-phase HPLC. HPLC was performed using a Shimadzu LC 10AD pump, a 712 WISP autosampler, a Waters Nova-Pak C18 column (3.9 × 150 mm), and a Waters 486 tunable absorbance detector (λ = 220 nm) at 35 °C by the elution of an acetonitrile and water mixture (55:45 vol %). The retention times of TEMPO, PEBr, biphenyl, PESG1A, PESG1B, and PETEMPO were 3.6, 6.0, 8.8, 44.2, 58.6, and 67.0 min, respectively. The data were collected and processed with a Shimadzu Class VP chromatographic data system (version 4.2).

Cyclic Voltammetric Measurements. Cyclic voltammetry was performed at room temperature using a Princeton Applied Research model 273 potentiostat/galvanostat instrument controlled with a personal computer and EG&G supplied software. Experiments were carried out in acetonitrile under argon in a three-compartment cell. The counter electrode was a platinum coil. The reference was a sodium chloride saturated calomel electrode (SSCE). A platinum electrode of 1 mm diameter was used as the working electrode. The scan rate ranged between 50 and 500 mV s^{-1}. The concentration of the copper complexes was kept at 0.01 M in all measurements with a electrolyte concentration of 0.1 M $[NBu_4][PF_6]$ in 5 mL of acetonitrile.

Acknowledgment. The authors acknowledge the Industrial Members of the ATRP Consortium at Carnegie Mellon University for the financial support of this research. B.G. is thankful for a fellowship of the DFG, Germany. We gratefully appreciate the donation of SG1 of Elf Atochem. We thank Jian Qiu and Jianhui Xia for helpful discussions.

References and Notes

(1) *Controlled Radical Polymerization*; Matyjaszewski, K., Ed.; American Chemical Society: Washington, DC, 1998; ACS Symp. Ser. Vol. 685.
(2) *Controlled/Living Radical Polymerization: Progress in ATRP, NMP and RAFT*; Matyjaszewski, K., Ed.; American Chemical Society: Washington, DC, 2000; ACS Symp. Ser. Vol. 768.
(3) Matyjaszewski, K. *Chem. Eur. J.* **1999**, *5*, 3095−3102.
(4) Patten, T. E.; Matyjaszewski, K. *Adv. Mater.* **1998**, *10*, 901.
(5) Patten, T. E.; Matyjaszewski, K. *Acc. Chem. Res.* **1999**, *32*, 895−903.
(6) Wang, J.-S.; Matyjaszewski, K. *Macromolecules* **1995**, *28*, 7901−7910.
(7) Wang, J.-S.; Matyjaszewski, K. *J. Am. Chem. Soc.* **1995**, *117*, 5614−5615.
(8) Patten, T. E.; Xia, J.; Abernathy, T.; Matyjaszewski, K. *Science* **1996**, *272*, 866−868.
(9) Matyjaszewski, K.; Patten, T. E.; Xia, J. *J. Am. Chem. Soc.* **1997**, *119*, 674−680.
(10) Xia, J.; Matyjaszewski, K. *Macromolecules* **1997**, *30*, 7697−7700.
(11) Qiu, J.; Matyjaszewski, K. *Macromolecules* **1997**, *30*, 5643−5648.
(12) Xia, J.; Gaynor, S. G.; Matyjaszewski, K. *Macromolecules* **1998**, *31*, 5958−5959.
(13) Coca, S.; Jasieczek, C. B.; Beers, K. L.; Matyjaszewski, K. *J. Polym. Sci., Part A: Polym. Chem.* **1998**, *36*, 1417−1424.
(14) Xia, J.; Matyjaszewski, K. *Macromolecules* **1999**, *32*, 2434−2437.
(15) Xia, J.; Zhang, X.; Matyjaszewski, K. *Macromolecules* **1999**, *32*, 3531−3533.
(16) Beers, K. L.; Boo, S.; Gaynor, S. G.; Matyjaszewski, K. *Macromolecules* **1999**, *32*, 5772−5776.
(17) Matyjaszewski, K.; Jo, S. M.; Paik, H.-j.; Shipp, D. A. *Macromolecules* **1999**, *32*, 6431−6438.
(18) Kickelbick, G.; Matyjaszewski, K. *Macromol. Rapid Commun.* **1999**, *20*, 341−346.
(19) Teodorescu, M.; Matyjaszewski, K. *Macromol. Rapid Commun.* **2000**, *21*, 190−194.
(20) Göbelt, B.; Matyjaszewski, K. *Macromol. Chem. Phys.* **2000**, *201*, 1619−1624.
(21) Percec, V.; Barboiu, B. *Macromolecules* **1995**, *28*, 7970.
(22) Percec, V.; Barboiu, B.; Neumann, A.; Ronda, J. C.; Zhao, M. *Macromolecules* **1996**, *29*, 3665.
(23) Haddleton, D. M.; Jasieczek, C. B.; Hannon, M. J.; Shooter, A. J. *Macromolecules* **1997**, *30*, 2190.
(24) Haddleton, D. M.; Crossman, M. C.; Dana, B. H.; Duncalf, D. J.; Heming, A. M.; Kukulj, D.; Shooter, A. J. *Macromolecules* **1999**, *32*, 2110.
(25) DiRenzo, G. M.; Messerschmidt, M.; Mülhaupt, R. *Macromol. Rapid Commun.* **1998**, *19*, 381−384.
(26) Destarac, M.; Bessiers, J.-M.; Boutevin, B. *Macromol. Rapid Commun.* **1997**, *18*, 1−8.

(27) Xia, J.; Zhang, X.; Matyjaszewski, K. *ACS Symp. Ser.* **1999**, *760*, 207.
(28) Matyjaszewski, K. *ACS Symp. Ser.* **1998**, *685*, 275.
(29) Fischer, H. *J. Polym. Sci., Part A: Polym. Chem.* **1999**, *37*, 1885−1901.
(30) Xia, J. Ph.D. Thesis, Carnegie Mellon University, 1999.
(31) Matyjaszewski, K.; Woodworth, B. E.; Zhang, X.; Gaynor, S. G.; Metzner, Z. *Macromolecules* **1998**, *31*, 5955−5957.
(32) Ohno, K.; Goto, A.; Fukuda, T.; Xia, J.; Matyjaszewski, K. *Macromolecules* **1998**, *31*, 2699−2701.
(33) Skene, W. G.; Belt, S. T.; Connolly, T. J.; Hahn, P.; Scaiano, J. C. *Macromolecules* **1998**, *31*, 9103−9105.
(34) Kothe, T.; Marque, S.; Martschke, R.; Popov, M.; Fischer, H. *J. Chem. Soc., Perkin Trans. 2* **1998**, *7*, 1553−1559.
(35) Goto, A.; Fukuda, T. *Macromol. Rapid Commun.* **1999**, *20*, 633−636.
(36) Paik, H.-j.; Matyjaszewski, K. *Polym. Prepr. (Am. Chem. Soc., Div. Polym. Chem.)* **2000**, *41* (1), 740−741.
(37) Chambard, G.; Klumperman, B.; German, A. L. *Macromolecules* **2000**, *33*, 4417−4421.
(38) Matyjaszewski, K.; Davis, K.; Patten, T. E.; Wei, M. *Tetrahedron* **1997**, *53*, 15321−15329.
(39) Li, I.; Howell, B. A.; Matyjaszewski, K.; Shigemoto, T.; Smith, P. B.; Priddy, D. B. *Macromolecules* **1995**, *28*, 6692−6693.
(40) Ohno, K.; Tsujii, Y.; Fukuda, T. *Macromolecules* **1997**, *30*, 2503−2506.
(41) Ando, T.; Kamigaito, M.; Sawamoto, M. *Tetrahedron* **1997**, *53*, 15445.
(42) Wang, J.-L.; Grimaud, T.; Shipp, D. A.; Matyjaszewski, K. *Macromolecules* **1998**, *31*, 1527.
(43) Chateauneuf, J.; Lusztyk, J.; Ingold, K. U. *J. Org. Chem.* **1988**, *53*, 1629−1632.
(44) Beckwith, A. L. J.; Bowry, V. W.; Ingold, K. U. *J. Am. Chem. Soc.* **1992**, *114*, 4983−4992.
(45) Mercier, C. L.; Lutz, J.-F.; Marque, S.; Moigne, F. L.; Tordo, P.; Lacroix-Desmaze, P.; Boutevin, B.; Couturier, J.-L.; Guerret, O.; Martschke, R.; Sobek, J.; Fischer, H. *ACS Symp. Ser.* **2000**, *768*, 108.
(46) It was noted that, during the HPLC analysis of reaction mixture, a minor side reaction was observed, resulting in partial decomposition of PEBr (20%). However, this decomposition was taken into account by the calibration of PEBr prepared under the identical analytical conditions, and the measured rate constant values were not affected.
(47) Skene, W. G.; Scaiano, J. C.; Listigovers, N. A.; Kazmaier, P. M.; Georges, M. K. *Macromolecules* **2000**, *33*, 5065−5072.
(48) Matyjaszewski, K. *Macromolecules* **1998**, *31*, 4710.
(49) Qiu, J.; Matyjaszewski, K.; Thouin, L.; Amatore, C. *Macromol. Chem. Phys.* **2000**, 1625−1631.
(50) Bard, A. J.; Faulker, L. R. *Electrochemical Methods*; John Wiley & Sons: New York, 1980.
(51) Koelle, U.; Khovzami, F. *Angew. Chem., Int. Ed. Engl.* **1980**, *19*, 640−641.
(52) Ambundo, E. A.; Deydier, M.-V.; Grall, A. J.; Aguera-Vega, N.; Dressel, L. T.; Cooper, T. H.; Heeg, M. J.; Ochrymowycz, L. A.; Rorabacher, D. B. *Inorg. Chem.* **1999**, *38*, 4233−4242.
(53) Kickelbick, G.; Reinohl, U.; Ertel, T. S.; Bertangnolli, H.; Matyjaszewski, K. *ACS Symp. Ser.* **2000**, *768*, 211.
(54) Rossi, A. R.; Hoffmann, R. *Inorg. Chem.* **1975**, *14*, 365−374.
(55) Hathaway, B. J. In *Comprehensive Coordination Chemistry*; Wilkinson, G., Ed.; Pergamon Books Ltd.: Oxford, 1987; Vol. 5, pp 652 and 697.
(56) tom Dieck, H.; Franz, K.-D.; Hohmann, F. *Chem. Ber.* **1975**, *108*, 163−173.

MA001181S